Diamond & Related Materials 60 (2015) 60–65

Contents lists available at ScienceDirect

Diamond & Related Materials

journal homepage: www.elsevier.com/locate/diamond

Nanometer-scale isotope analysis of bulk diamond by atom probe tomography

R. Schirhagl [a,b,*], N. Raatz [c], J. Meijer [c], M. Markham [d], S.S.A. Gerstl [e], C.L. Degen [a,**]

[a] Department of Physics, ETH Zurich, Otto Stern Weg 1, 8093 Zurich, Switzerland
[b] University Medical Center Groningen, Groningen University, Department of Biomedical Engineering, Antonius Deusinglaan, 1, 97 13 AV Groningen, The Netherlands
[c] Department Nuclear Solid State Physics, Universität Leipzig, Linnestr. 5, D-04103 Leipzig, Germany
[d] Element Six Ltd, Global Innovation Centre, Fermi Avenue, Didcot OX11 0 QR, United Kingdom
[e] ScopeM, ETH Zurich, Auguste Piccard Hof 1, 8093 Zurich, Switzerland

ARTICLE INFO

Article history:
Received 27 July 2015
Received in revised form 19 October 2015
Accepted 19 October 2015
Available online 21 October 2015

Keywords:
Single crystal diamond
Atom probe tomography
Nanoscale analysis
Isotope analysis
Doping
Depth profile

ABSTRACT

Atom-probe tomography (APT) combines field emission of atoms with mass spectrometry to reconstruct three-dimensional tomograms of materials with atomic resolution and isotope specificity. Despite significant recent progress in APT technology, application to wide-bandgap materials with strong covalent bonds has remained challenging or low yielding. Here we report APT measurements on bulk diamond grown by chemical vapor deposition. Using a conductive substrate in combination with laser-pulsing, carbon atoms could be controllably field evaporated and tomograms containing up to 6 million atoms could be reconstructed. We have subsequently applied the technique to iage the depth distribution of a sub-surface nitrogen δ-layer with nanometer spatial resolution. With future development, the technique may enable detailed characterization of dopants in diamond at an atomic level, which would be of great interest to the many scientific and industrial applications exploiting the unique properties of the material.

1. Introduction

Doping of diamond is important for many emerging technologies that attempt to exploit the materials' remarkable properties in high-end electronic devices and sensors. For example, doping of diamond by phosphorus or boron introduces donors or acceptors that can turn insulating into semiconducting diamond [1], with potential applications in high-power diodes or transistors. Boron-doped diamond is also a candidate electrode material for next generation, highly stable and accurate pH sensors [2] and a range of other electrochemical applications [3]. Optically bright defects, such as the silicon vacancy (SiV) or the nitrogen vacancy (NV) color centers, hold promise as single photon emitters in photonic networks [4]. NV centers are moreover beginning to be utilized as nanoscale probes for magnetic and electric fields, or temperature, with potential uses in sensor arrays or high-resolution magnetic imaging [5]. In most of these applications, it is crucial that defects or dopants can be precisely positioned within tens of nanometers, and sometimes within a few nanometers from a diamond surface.

Controlled vertical placement of foreign atoms is possible both by ion implantation and by *in-situ* growth using chemical vapor deposition (CVD). For ion implantation, the penetration depth can be approximately chosen by adjusting the ion acceleration voltage, and surface proximities of a few nm have been realized for low (<10 keV) implantation energies [6,7]. The placement of defects, however, is stochastic and the peak depth and distribution can only be predicted by Monte Carlo or molecular dynamics simulations [8]. Although these simulations are extremely useful, they usually neglect effects like channeling, tilt of crystallographic planes, or surface potential build up, and thus are approximate at best. *In-situ* growth by CVD overcomes these issues by temporarily adding the dopant precursor to the feed gas, and surface layers or interlayers as thin as 5 nm have been reported [9,10,11]. Achieving precise thicknesses and absolute placement of such δ-layers of high foreign atom concentration, however, remains challenging because growth rates for thin layers are difficult to control and calibrate [12].

An important obstacle to controlled shallow defect generation is the lack of suitable analytical tools that can experimentally verify defect depths or lateral placement. Secondary ion mass spectrometry (SIMS) has been used to study diamond [12,13] and to investigate nitrogen contents [14,15], but depth resolutions are typically >10 nm and large, homogeneous surface areas are required. SIMS is especially problematic for obtaining information on insulating materials, like diamond, due to charge build-up and other artifacts [14]. For nitrogen, which is the target dopant in this study, SIMS is additionally hampered because the species does not form stable negative ions in isolation, such that ionization efficiencies and yields are low. Other techniques include non-Rutherford

* Correspondence to: R. Schirhagl, Department of Physics, ETH Zurich, Otto Stern Weg 1, 8093 Zurich, Switzerland.
** Corresponding author.
E-mail addresses: r.schirhagl@umcg.nl (R. Schirhagl), degenc@ethz.ch (C.L. Degen).

http://dx.doi.org/10.1016/j.diamond.2015.10.016
0925-9635/

backscattering spectroscopy or elastic recoil detection analysis [16], but also these require large sample areas. For the specific case of NV color centers, depth measurements have also been reported using fluorescence quenching [17] and spin relaxometry [18,19,11]. In this study, we explore whether atom probe tomography [20] could serve as a method for analyzing atomic defects in bulk diamond with nanometer spatial resolution.

Atom probe tomography (APT) combines field evaporation of ions with time-of-flight (TOF) mass spectrometry to obtain three-dimensional tomograms of materials with sub-nanometer resolution and isotope specificity. In APT, the material under investigation is sculpted into a nanoscale tip and ions are evaporated by voltage pulses that create extremely high local electric fields (typically 10s of V/nm). Since ion emission is directional, a three-dimensional tomogram can be reconstructed (see Fig. 1A). The method thus avoids limitations imposed by SIMS, including the requirement of a large, uniform surface area, and it has inherently higher spatial resolution. The main challenges with APT of ceramics and dielectrics, like diamond, are the presence of strong covalent bonds and the fact that these are electrical insulators. Although successful APT has been reported for, *e.g.*, alumina [21], silicon carbide [22], and zinc oxide [23] the precise mechanistics of atom emission in these materials is only partially understood [23,24]. Diamond is especially challenging because carbon has the highest evaporation field (>100 V/nm) of any element [25] and because the material has a large bandgap (E_{Gap} = 5.5 eV) that remains unaffected even at the sub-nanometer scale [26]. Pioneering work with diamond-like materials has been carried out by Nishikawa and coworkers in the late 1990s using a scanning atom probe [27,28]. More recently, APT has been applied to meteoritic nanodiamonds embedded in a platinum matrix [29], and initial measurements on thin diamond films grown by chemical vapor deposition (CVD) have been reported [30].

In this work, we discuss APT measurements of bulk single crystal diamond. We find that the adverse material properties of diamond can be overcome by the use of a conductive diamond substrate in combination with high-energy laser pulsing. APT runs with up to 6 million atoms could be reconstructed, eventually limited by tip rupture, and the associated mass spectra consistently reproduced the correct ^{12}C-to-^{13}C ratio of naturally occurring carbon isotopes. Although rather high laser-pulsing energies of typically 500 pJ were required to achieve stable and sufficiently high ion count rates, we found carbon to evaporate smoothly and controllably in the diamond phase. We have subsequently applied APT to image the depth distribution of a ~6 nm nitrogen δ-layer created by ion implantation, in reasonable agreement with Monte Carlo simulations. The AP tomogram further showed indications of local clustering of nitrogen and displayed no signs of ion channeling.

2. Materials and methods

The substrate used in this study was a bulk piece of boron-doped (~100 ppm) diamond grown by chemical vapor deposition. The as-grown polycrystalline diamond had a predominately (111) orientated surface. The surface was subsequently mechanically polished to a surface roughness of about 1 nm-rms as measured by atomic force microscopy. The crystallite size was 10–50 μm at the investigated surface. Since this was much larger than finished APT probe tip diameters (~50 nm), the defect-rich grain boundaries were avoided and single-crystal behavior could be assumed. The boron doping served to enhance the electrical conductivity of the diamond.

Tips were prepared by focused ion beam (FIB) milling and subsequent transfer to a sample post [31]. For some of the tips, the diamond surface was coated by 3 nm of titanium and ~50 nm of platinum before FIB milling. The Ti was deposited by e-beam evaporation and served as a fiducial layer referencing the diamond surface, while the Pt was accumulated by gas-assisted FIB deposition and served to minimize unwanted Ga ion implantation and substrate damage. We found during APT analysis that the Pt/Ti protection was efficient, and only very little Ga penetrated into the diamond. Moreover, no indications of tip damage by the Ga were seen even in unprotected diamond tips. In order to form sharp tips suitable for field emission, a triangular wedge was carved out of the diamond surface using a focused ion beam (FIB) and then transferred by a micromanipulator to a sample post. The triangular subunits of the wedge were then sculpted by FIB, using annular mill patterns, into needle-like geometries of ~50 nm apex diameter. A scanning electron micrograph of a finished tip is shown in Fig. 1B and a sketch of the layered tip structure is shown in Fig. 1C. Additional details on tip preparation by FIB are given as Supplementary Information.

The samples were analyzed in a Cameca LEAP 4000X-HR instrument in pulsed laser mode at 100 K specimen temperature. The laser pulses (λ = 355 nm, focused to a < 3 μm spot size) were applied at a rate of 160 kHz to the specimen apex in order to obtain a C^{++}/C^{+} charge state ratio of 0.85. The energy per pulse was not accessible with this instrument; we estimate it at around 500 pJ distributed over a Gaussian spot of ~3 μm diameter. We have initially tried lower pulse energies, but found that high pulse powers were essential for achieving stable evaporation at sufficiently high rates. The high pulse energy led to an increased background noise and possibly surface diffusion of Ti and Pt in metal-capped tips (see Results and discussion). Detection rates were ~0.5 ions per 100 laser pulses at a ratio of about 80% single detector hits and 20% multiples. Of about 50 tips fabricated, 15 yielded mass spectra and all of them were reconstructed. Not all analyses produced meaningful results, either because of early tip rupture or because tip diameters were too large.

The data were reconstructed using IVAS 3.6.8 software by correlating to the best known pre-run tip geometries and concentration gradients in the reference layer. (Post-run geometries were not available as an APT run was typically continued until a tip spontaneously ruptured). Reconstruction of the vertical *z* position was based on the temporal sequence of detection events. Due to the significant number of multiplicity events and cluster emissions especially in the sacrificial Pt layer, the overall vertical scaling was difficult to establish. We have

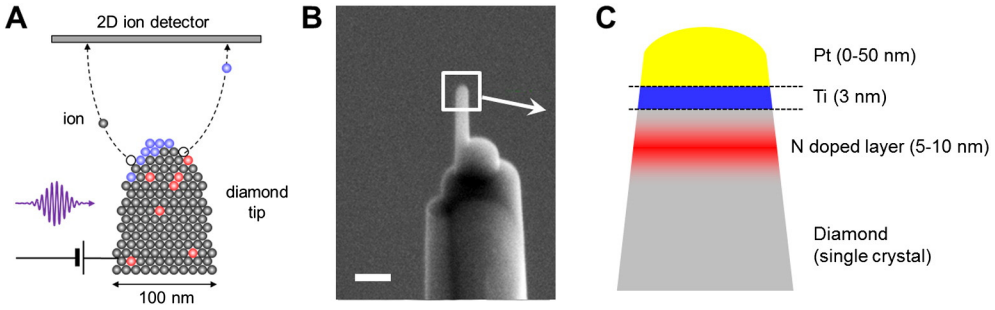

Fig. 1. (A) Principle of atom probe tomography (APT). The material under investigation, here surface-doped bulk diamond grown by chemical vapor deposition (CVD), is structured into a nanoscale tip. A combination of high voltage and UV laser pulses is used to evaporate atoms one-by-one and to record their original position using a two-dimensional ion detector. The temporal sequence of detection events then allows for reconstructing the three-dimensional position. Ion detection is coupled to a time-of-flight (TOF) mass spectrometer for isotope identification. (B) Scanning electron micrograph of a finished single-crystal diamond tip. Scale bar is 200 nm. (C) Sketch of the layered structure of a diamond tip with nitrogen δ-doping.

therefore used the 3-nm fiducial Ti layer and the onset of the diamond carbon as an independent way of ranging the data (see Supplementary Fig. 2). The two scales were in reasonable agreement; for the tip analyzed in Figs. 4, 5 below, the reconstruction yielded at diamond thickness of ~30 nm while the Ti ranging resulted in ~22 nm. Overall we estimate a vertical *z*-scaling error of about 2×.

The reconstructed three-dimensional data set was finally decomposed into isotope-specific tomograms using the TOF information. The analyzed peaks and isotopes are collected in Table 1.

For the nitrogen dopant study, the diamond was implanted with $^{14}N^+$ ions at an energy of 5 keV and a fluence of 10^{15} cm^{-2} in localized spots of ~100 μm radius [6,7]. This implantation energy is expected to create a doping layer approximately 8 nm below the surface, with a width of ~6 nm due to vertical straggling. Simulations of ion implantation were carried out using the stopping range of ions in matter (SRIM) software package [8]. The implanted ion was N^+ with an atomic weight of 14 u, an energy of 5 keV, and an impinging angle of 0° (vertical). The simulated target used carbon at a density of 3.157 g/cm^3, a surface energy of 7.41 eV, a displacement energy of 37.5 eV [33] and a binding energy of 31.6 eV [34].

3. Results and discussion

Since APT has, to the best of our knowledge, never been applied to bulk and single crystalline diamond, we have in a first step investigated whether controlled and consistent evaporation of carbon ions can be established. Fig. 2 presents an APT run with $2.0 \cdot 10^6$ detection events obtained from a tip that only contained diamond carbon. The APT tomogram and the derived vertical carbon concentration profiles are clearly smooth, which indicates that atoms were stably evaporated despite of the high laser pulse energy. The stable evaporation behavior in the diamond region can be corroborated by looking at the ion detection rate and tip bias voltage (see Supplementary Fig. 3). The vertical concentration profiles of this and two other tips (Supplementary Fig. 4) also show that Ga implantation from the FIB milling is small and confined to the top ~10 nm, with no discernible damage to the diamond tip.

We next turn our attention to a nitrogen-doped tip, as sketched in Fig. 1C. The investigated tip included the Ti and Pt capping layers deposited for surface referencing and tip protection. Fig. 3 presents the APT mass spectrum of a tip with $6.3 \cdot 10^6$ detection events. As expected, the mass spectrum showed peaks for carbon, nitrogen, titanium, platinum, and possibly boron. Beside the simple atomic ions, a number of additional peaks reflecting higher charge states and molecular ions, as well as hydrogen, were observed. These peaks are a result of the high laser pulse energy and residual gas in the APT chamber. Despite of the rather crowded mass spectrum, most elements of interest could be uniquely identified *via* peak multiplets of naturally occurring isotopes (Fig. 3B–E). Table 1 shows that integrated peak intensities are in excellent agreement with the isotope abundance (see Table 1) such that accidental peak overlap can be excluded. For nitrogen ^{14}N, where no isotope comparison was possible, we confirmed the peak by a control run from an all-diamond tip that did not contain any nitrogen (Fig. 3C).

A tomographic reconstruction of the tip is shown in Fig. 4. As expected, the tomogram showed a distinct upper and lower region, rich in Pt (yellow) and C (black), respectively. These regions reflect the sacrificial surface layer and the diamond bulk, respectively. The diamond region further included significant amounts of N, Ti and Pt.

Although the Pt and diamond regions were well-resolved, the separation between layers was rather poor and cross-contamination of C, Ti, Pt and N was visible. The large amount of C in the Pt region is due to the metal-organic vapor precursor used for deposition [22,35], while N contamination is due to residual gas in the chamber. The Pt region additionally showed localized granules. These signatures are well-known for FIB-deposited Pt [35] and probably exacerbated by the high laser pulse energy. It is also known that high pulse energies can lead to tip damage [36] and atomic diffusion on the tip surface [37]. The latter effect would well explain the apparent contamination of the diamond region by Ti; as soon as the atom evaporation reaches the Ti layer, diffusion of Ti atoms down the diamond shaft occurs, leading to a long vertical tail in the Ti concentration profile (see Suppl. Fig. 5).

The diamond region, by contrast, showed a smooth evaporation behavior, corroborating the run with the all-diamond tip analyzed in Fig. 2. Inspection of the ion sequence number, detection event histogram and an alternative reconstruction confirmed this picture (see Supplementary Figs. 3 and 5).

We now focus on the nitrogen distribution in the diamond region, shown in Fig. 5. The N concentration clearly showed a vertical variation that was peaked about 6 nm below the Ti reference layer (Fig. 5B), consistent with the doping layer introduced by the ion implantation. The vertical concentration profile of N, obtained by integrating over the horizontal cross-section of the three-dimensional tomogram, could be fit by a Gaussian profile with a maximum concentration of about 0.7% and a linewidth (2σ) of roughly 10 nm. We have compared these values with a SRIM simulation, plotted in Fig. 5D. The simulation predicted a peak depth of 8 nm and a linewidth of 7 nm. Since the vertical scaling of the APT tomogram is not precisely known (see Materials and methods), the simulation is in remarkably good agreement with the APT result.

We finally discuss two noteworthy features of the three-dimensional tomogram and the vertical concentration profile. Firstly, the nitrogen tomogram showed measurable density fluctuations, visible in the zoomed region in Fig. 3C. The "bunching" of atoms was most obvious at the upper edge that was closest to the surface, while the deeper region was much more homogeneous. The origin of clusters is presently unclear; we believe that they were either created during nitrogen ion implantation, were due to a chemical reaction of diamond with Ti assisted by the laser pulse, or were related to residual surface roughness (~1 nm-rms).

A second interesting observation is the absence of ion channeling. For ion implantation into crystalline solids at sufficiently high kinetic energy, it is well established that ions can channel along crystal planes and travel much deeper into the material than expected from SRIM simulations. This results in a deep tail in the dopant concentration. Ion channeling in diamond has been experimentally observed by SIMS measurements of a deeper (10–30 keV) doped diamond substrate [15]. By contrast, our measurements with low energy (5 keV) ions showed a Gaussian depth profile with no deep tail, providing no

Table 1
List of analyzed peaks and corresponding isotopes. Literature values of natural isotope abundance are according to Ref. [32]. Experimental values were obtained by peak integration (±0.5 u/e) from the mass spectrum shown in Fig. 3. For titanium, only the Ti^{2+} charge state was analyzed as almost no Ti^+ was detected.

Isotope	Analyzed charge state	Peak at	Isotope abundance — literature value	Isotope abundance — this study
^{10}B	+1	10 u/e *	20%	–
^{11}B	+1	11 u/e	80%	–
^{12}C	+1	12 u/e	1.1%	1.4%
^{13}C	+1	13 u/e	99%	99%
^{14}N	+1	14 u/e	99.6%	–
^{46}Ti	+2	23 u/e	8.2%	7.3%
^{47}Ti	+2	23.5 u/e	7.4%	6.4%
^{48}Ti	+2	24.0 u/e **	74%	76%
^{49}Ti	+2	24.5 u/e	5.4%	4.9%
^{50}Ti	+2	25 u/e	5.2%	5.5%
^{192}Pt	+1	192 u/e	0.78%	0.82%
^{194}Pt	+1	194 u/e	33%	33%
^{195}Pt	+1	195 u/e	34%	33%
^{196}Pt	+1	196 u/e	25%	26%
^{198}Pt	+1	198 u/e	7.2%	7.9%

Notes: *The $^{10}B^+$ peak (expected at 10 u/e) was below the detection limit. **A significant contribution from $^{12}C_2^+$ to the 24 u/e peak can be excluded because the peak intensities of Ti isotopes agree with the natural abundances.

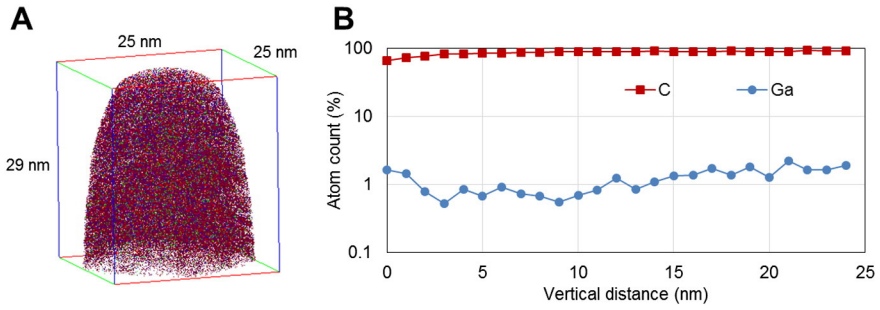

Fig. 2. (A) Reconstruction and (B) vertical concentration profile of carbon (dark red) and gallium (blue) for an all-diamond tip. The gallium was introduced during FIB milling. Carbon atom count includes higher charge states and multiples, but no hydrides or heteroatomic molecular ions. The baseline noise was about 1% using a one u/e integration window. (For interpretation of the references to color in this figure legend, the reader is referred to the web version of this article.)

evidence for ion channeling. Our observations thus support theoretical predictions suggesting that channeling becomes negligible at very low implantation energies [38].

4. Conclusions

In conclusion, we have performed an APT investigation of bulk, quasi-single-crystal diamond grown by chemical vapor deposition. By using a conductive, boron-doped substrate in combination with laser pulse assistance, we found that carbon atoms can be field evaporated in a smooth and controlled way from FIB-sculpted diamond tips. The mass spectra produced the correct isotope ratio for ^{12}C and ^{13}C and other detected elements, supporting the consistency of the measurements. The maximum ion count was limited to 2–6 · 10^6 due to spontaneous tip rupture, corresponding to an investigated vertical range of 10–30 nm. The threshold concentration level was ~3 · 10^{19} cm^{-3}. We have further used APT to measure the vertical concentration profile of a ~6 nm thick, nitrogen doped layer created by ion implantation, and found reasonable agreement with numerical simulations of the implantation. The three-dimensional tomogram furthermore revealed

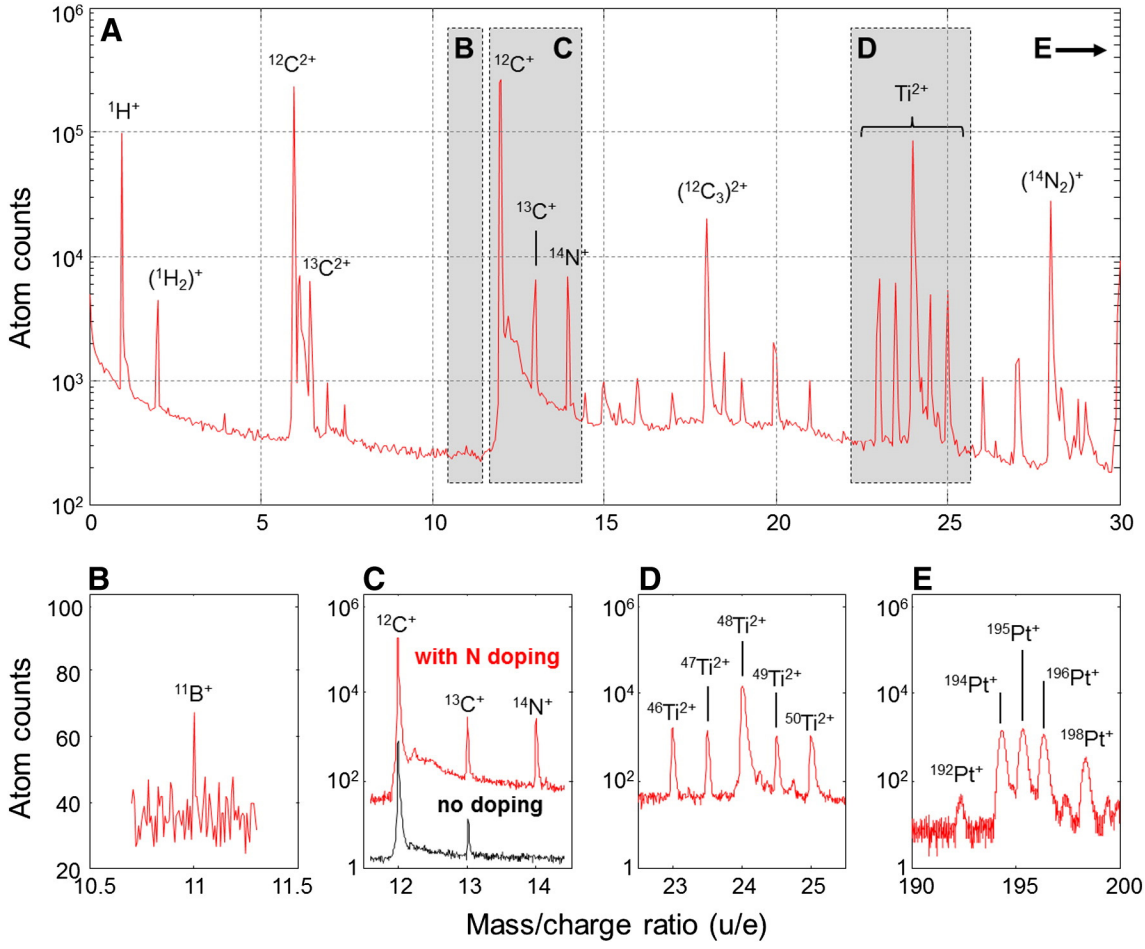

Fig. 3. (A) Mass spectrum of an APT dataset with 6.3 · 10^6 atoms. Peaks are assigned with the most likely atomic or molecular species. (B–E) High resolution spectra for all elements included in the APT reconstruction. The multiplets clearly reflect the ratios of naturally occurring isotopes summarized in Table 1. Nitrogen ^{14}N was confirmed using a control run with undoped (nitrogen-free) diamond using the peak at 14 u/e. Background counts correspond to ~10^{19} ions/cm^3 or ~50 ppm. Counts are binned into 0.03 u/e intervals for (A) and into 0.007 u/e intervals for (B–E).

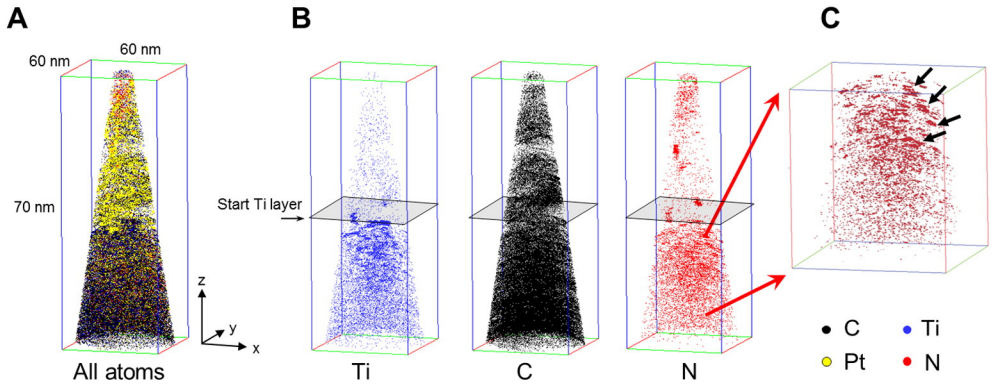

Fig. 4. (A) Shank-based reconstruction of a nitrogen-doped diamond tip similar to Fig. 1C. The shank angle was 13°. Only the inner core was analyzed in order to reduce the effects of tip curvature and discrepant evaporation behavior of the constituents. Each dot represents one atom. (B) Elemental analysis showing the distributions of titanium, carbon and nitrogen. A plane indicates the top edge of the 3 nm titanium reference layer. (C) Enlarged tomogram of the nitrogen-doped area, showing fluctuations in the local concentration (black arrows). A scanning electron micrograph and alternate reconstruction is shown in Supplementary Fig. 5. (For interpretation of the references to color in this figure, the reader is referred to the web version of this article.)

measurable density fluctuations especially in the near-surface region of the nitrogen doping layer, and showed no evidence for channeling during ion implantation.

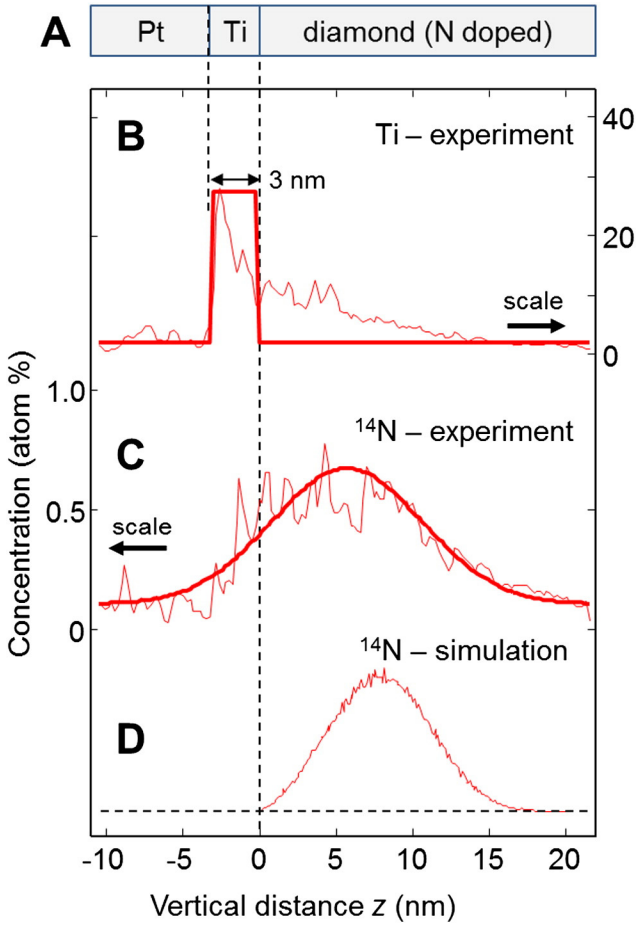

Fig. 5. (A) Sketch of the vertical layering of the Pt/Ti/bulk diamond interface region. (B) Vertical concentration of the Ti ranging layer and (C) of ^{14}N across the diamond interface region obtained by lateral integration over the AP tomogram of Fig. 3. Bold solid lines represent the 3-nm thick binary profile of Ti and a Gaussian fit to the ^{14}N concentration, respectively. The atomic concentration is probably underestimated, because not all peaks could be captured in the mass spectrum due to signal overlap. (D) Complementary SRIM simulation for $^{14}N^{+}$ ions implanted into diamond at 5 kV acceleration voltage as detailed in the Materials and methods section. The vertical profiles of all other isotopes are provided in Supplementary Fig. 3.

Our study demonstrates that APT can be controllably applied to bulk diamond. Looking forward, the method's ability to characterize defects at an atomic level would be very useful to the many scientific and industrial applications of diamond. For example, APT could in principle determine clusters, dislocations, inclusions or nanometer variations in doping levels [39]. At sufficiently low noise levels, a combination of field ion microscopy and APT could also detect atomic pairs and yield information on binding energies [40]. While in our study the rather high background noise inhibited such analyses, future improvements to APT technology or top-down etching of extremely sharp diamond needles [41] could help realizing these exciting applications.

Prime novelty statement

We report the successful application of atom probe tomography to bulk, single crystal diamond. As a pilot application, we show that a depth profile of a nitrogen doping layer created by ion implantation can be resolved with nanometer resolution.

Acknowledgments

This work has been supported by the European Commission through Project FP7-611143 DIADEMS, and by the Swiss National Science Foundation through Project 200021_137520/1 and the NCCR QSIT. R. S. acknowledges a Marie Curie Intraeuropean Fellowship (Project No. 130315).

Appendix A. Supplementary data

Supplementary data to this article can be found online at http://dx.doi.org/10.1016/j.diamond.2015.10.016.

References

[1] A. Aleksov, A. Vescan, M. Kunze, P. Gluche, W. Ebert, E. Kohn, A. Bergmaier, G. Dollinger, Diamond junction FETs based on delta-doped channels, Diamond Relat. Mater. 8 (1999) 941–945.
[2] A. Denisenko, G. Jamornmarn, H. El-Hajj, E. Kohn, pH sensor on O-terminated diamond using boron-doped channel, Diamond Relat. Mater. 16 (2007) 905–910.
[3] J.V. Macpherson, A practical guide to using boron doped diamond in electrochemical research, Phys. Chem. Chem. Phys. 17 (2015) 2935–2949.
[4] I. Aharonovich, S. Castelletto, D.A. Simpson, C.H. Su, A.D. Greentree, S. Prawer, Diamond-based single-photon emitters, Rep. Prog. Phys. 74 (2011) 076501.
[5] R. Schirhagl, K. Chang, M. Loretz, C.L. Degen, Nitrogen-vacancy centers in diamond: nanoscale sensors for physics and biology, Annu. Rev. Phys. Chem. 65 (2014) 83.
[6] S. Pezzagna, B. Naydenov, F. Jelezko, J. Wrachtrup, J. Meijer, Creation efficiency of nitrogen-vacancy centres in diamond, new, J. Phys. 12 (2010) 065017.
[7] B.K. Ofori-Okai, S. Pezzagna, K. Chang, M. Loretz, R. Schirhagl, Y. Tao, B.A. Moores, K. Groot-Berning, J. Meijer, C.L. Degen, Spin properties of very shallow nitrogen vacancy defects in diamond, Phys. Rev. B 86 (2012) 081406.

[8] J.F. Ziegler, M. Ziegler, J. Biersack, SRIM — the stopping and range of ions in matter, Nucl. Instrum. Methods Phys. Res. Sect. B 268 (2010) 1818–1823.
[9] K. Ohno, F.J. Heremans, L.C. Bassett, B.A. Myers, D.M. Toyli, A.C.B. Jayich, C.J. Palmstrom, D.D. Awschalom, Engineering shallow spins in diamond with nitrogen delta-doping, Appl. Phys. Lett. 101 (2012) 082413.
[10] K. Ohashi, T. Rosskopf, H. Watanabe, M. Loretz, Y. Tao, R. Hauert, S. Tomizawa, T. Ishikawa, J. Ishi-hayase, S. Shikata, C.L. Degen, K.M. Itoh, Negatively charged nitrogen-vacancy centers in a 5 nm thin 12C diamond film, Nano Lett. 13 (2013) 4733–4738.
[11] B.A. Myers, M.C. Dartiailh, K. Ohno, A. Das, D.D. Awschalom, A.C. Bleszynski Jayich, Probing surface noise with depth-calibrated spins in diamond, Phys. Rev. Lett. 113 (2014) 027602.
[12] A. Fiori, F. Jomard, T. Teraji, S. Koizumi, J. Isoya, E. Gheeraert, E. Bustarret, Synchronized B and 13C diamond delta structures for an ultimate in-depth chemical characterization, Appl. Phys. Express 6 (2013) 045801.
[13] R. Steiner, G. Stingeder, H. Hutter, M. Grasserbauer, R. Haubner, B. Lux, Imaging SIMS for the investigation of substrate surfaces for CVD diamond deposition, Fresenius J. Anal. Chem. 352 (1995) 313–317.
[14] D. Zhou, F.A. Stevie, L. Chow, J. McKinley, H. Gnaser, V.H. Desai, Nitrogen incorporation and trace element analysis of nanocrystalline diamond thin films by secondary ion mass spectrometry, J. Vac. Sci. Technol. A 17 (1999) 1135.
[15] D.M. Toyli, C.D. Weis, G.D. Fuchs, T. Schenkel, D.D. Awschalom, Chip-scale nanofabrication of single spins and spin arrays in diamond, Nano Lett. 10 (2010) 3168–3172.
[16] E. Garratt, S. Al Faify, D.P. Cassidy, A. Dissanayake, D.C. Mancini, M.K. Ghantasala, A. Kayani, Depth profiling of nitrogen within 15N-incorporated nano-crystalline diamond thin films, Appl. Phys. Lett. 103 (2013) 131602.
[17] J. Tisler, T. Oeckinghaus, R.J. Stohr, R. Kolesov, R. Reuter, F. Reinhard, J. Wrachtrup, Single defect center scanning near-field optical microscopy on graphene, Nano Lett. 13 (2013) 3152–3156.
[18] M. Loretz, S. Pezzagna, J. Meijer, C.L. Degen, Nanoscale nuclear magnetic resonance with a 1.9-nm-deep nitrogen-vacancy sensor, Appl. Phys. Lett. 104 (2014) 33102.
[19] T. Rosskopf, A. Dussaux, K. Ohashi, M. Loretz, R. Schirhagl, H. Watanabe, S. Shikata, K.M. Itoh, C.L. Degen, Investigation of surface magnetic noise by shallow spins in diamond, Phys. Rev. Lett. 112 (2014) 147602.
[20] T. Kelly, M. Miller, Invited review article: atom probe tomography, Rev. Sci. Instrum. 78 (2007) 031101.
[21] E.A. Marquis, N.A. Yahya, D.J. Larson, M.K. Miller, R.I. Todd, Probing the improbable: imaging carbon in alumina, Mater. Today 13 (2010) 42.
[22] M. Miller, P. Angelini, A. Cerezo, K. More, Pulsed laser atom probe characterization of silicon carbide, J. Phys. Colloq. 50 (1989) C8–459.
[23] L. Mancini, N. Amirifar, D. Shinde, I. Blum, M. Gilbert, A. Vella, F. Vurpillot, W. Lefebvre, R. Lardé, E. Talbot, P. Pareige, X. Portier, A. Ziani, C. Davesnne, C. Durand, J. Eymery, R. Butté, J. Carlin, N. Grandjean, L. Rigutti, Composition of wide bandgap semiconductor materials and nanostructures measured by atom probe tomography and its dependence on the surface electric field, J. Phys. Chem. C 118 (2014) 24136–24151.
[24] M. Karahka, H. Kreuzer, Field Evaporation of Insulators and Semiconductors: Theoretical Insights for ZnO, Ultramicroscopy, 2015 (in press).
[25] T.T. Tsong, Field ion image formation, Surf. Sci. 70 (1978) 211.
[26] F.M. Hossain, M.W. Doherty, H.F. Wilson, L.C.L. Hollenberg, Ab initio electronic and optical properties of the N-V- center in diamond, Phys. Rev. Lett. 101 (2008) 226403.
[27] O. Nishikawa, T. Sekine, Y. Ohtani, K. Maeda, Y. Numada, M. Watanabe, Atomic investigation of individual apexes of diamond emitters by a scanning atom probe, J. Vac. Sci. Technol. B 16 (1998) 836–840.
[28] O. Nishikawa, Y. Ohtani, K. Maeda, M. Watanabe, K. Tanaka, Atom-by-atom analysis of diamond graphite and vitreous carbon by the scanning atom probe, J. Vac. Sci. Technol. B 18 (2000) STM-660.
[29] F.J. Stadermann, D. Isheim, X. Zhao, T.L. Daulton, C. Floss, D.N. Seidman, P.R. Heck, M.J. Pellin, M.R. Savina, J. Hiller, A. Mane, J. Elam, A.M. Davis, T. Stephan, S. Amari, Atom-probe tomographic characterization of meteoritic nanodiamonds and presolar SiC, Lunar Planet. Sci. 4 (2011) 1595.
[30] T.L. Martin, P.W. May, P.A.J. Bagot, M.P. Moody, Mapping of dopant atoms in CVD diamond films using atom probe tomography, MRS Fall Meeting, Boston, Abstract R8.07, 2014.
[31] M.K. Miller, K.F. Russell, G.B. Thompson, Strategies for fabricating atom probe specimens with a dual beam FIB, Ultramicroscopy 102 (2005) 287–298.
[32] J.R. De Laeter, J.K. Böhlke, P. De Bievre, H. Hidaka, H.S. Peiser, K.J.R. Rosman, P.D.P. Taylor, Atomic weights of the elements, Pure Appl. Chem. 75 (683) (2003).
[33] J. Koike, D.M. Parkin, T.E. Mitchell, Displacement threshold energy for type IIa diamond, Appl. Phys. Lett. 60 (1992) 1450.
[34] M.H. Nazare, A.J. Neves, Properties, growth an applications of diamond, Emis Datareviews Series, 26, The Institution of Engineering and Technology, 2000.
[35] S.S.A. Gerstl, A. Morrone, R. Kvitek, Three-dimensional nanoscale characterization of Pt deposition from an organometallic precursor induced by a focused ion beam, Microsc. Microanal. 12 (S2) (2006) 1252–1253.
[36] J. Bogdanowicz, M. Gilbert, N. Innocenti, S. Koelling, B. Vanderheyden, W. Vandervorst, Light absorption in conical silicon particles, Opt. Express 21 (2013) 3891–3896.
[37] G.L. Kellogg, Determining the field emitter temperature during laser irradiation in the pulsed laser atom probe, J. Appl. Phys. 52 (1981) 5320.
[38] P. Honicke, B. Beckhoff, M. Kolbe, D. Giubertoni, J. van den Berg, G. Pepponi, Depth profile characterization of ultra shallow junction implants, Anal. Bioanal. Chem. 396 (2010) 2825.
[39] D.J. Larson, et al., Local Electrode Atom Probe Tomography, Springer, New York, 2013 201.
[40] J. Liu, C.-W. Wu, T.T. Tsong, Measurement of the atomic site specific binding energy of surface atoms of metals and alloys, Surf. Sci. 246 (1991) 157–162.
[41] Y. Tao and C. L. Degen, submitted (2015).